Available online at www.sciencedirect.com
ScienceDirect
International Journal of Mass Spectrometry 260 (2007) 185–194
International Journal of Mass Spectrometry
www.elsevier.com/locate/ijms

Direct profiling of myelinated and demyelinated regions in mouse brain by imaging mass spectrometry

Ruben Ceuppens [a,1], Debora Dumont [b,1], Leen Van Brussel [a], Babs Van de Plas [a], Ruth Daniels [b], Jean-Paul Noben [b], Peter Verhaert [a,b,c], Estel Van der Gucht [a], Johan Robben [b], Stefan Clerens [a,2], Lutgarde Arckens [a,*]

[a] *Laboratory of Neuroplasticity and Neuroproteomics, K.U. Leuven, Naamsestraat 59, B-3000 Leuven, Belgium*
[b] *Hasselt University, Biomedical Research Institute (Biomed) and Transnationale Universiteit Limburg, School of Life Sciences, Diepenbeek, Belgium*
[c] *Laboratory for Analytical Biotechnology, Delft University of Technology, Delft, The Netherlands*

Received 15 June 2006; received in revised form 3 September 2006; accepted 5 September 2006
Available online 2 October 2006

Abstract

One of the newly developed imaging mass spectrometry (IMS) technologies utilizes matrix-assisted laser desorption/ionization (MALDI) mass spectrometry to map proteins in thin tissue sections. In this study, we evaluated the power of MALDI IMS as we developed it in our (Bruker) MALDI TOF (Reflex IV) and TOF-TOF (Ultraflex II) systems to study myelin patterns in the mouse central nervous system under normal and pathological conditions. MALDI IMS was applied to assess myelin basic protein (MBP) isoform-specific profiles in different regions throughout the mouse brain. The distribution of ions of *m/z* 14,144 and 18,447 displayed a striking resemblance with white matter histology and were identified as MBP isoform 8 and 5, respectively. In addition, we demonstrated a significant reduction of the MBP-8 peak intensity upon MALDI IMS analysis of focal ethidium bromide-induced demyelinated brain areas. Our MS images were validated by immunohistochemistry using MBP antibodies. This study underscores the potential of MALDI IMS to study the contribution of MBP to demyelinating diseases.

Keywords: MALDI IMS; Mouse; Brain; Myelin basic protein; Histology

Abbreviations: aca, anterior commissure; aci, intrabulbar anterior commissure; aptd, dorsal part of the anterior pretectal nucleus; cc, corpus callosum; cg, cingulum; cp, cerebral peduncle; CHCA, alpha-cyano-4-hydroxycinnamic acid; DAB, diaminobenzidine; dhc, dorsal horn of the hippocampus; dpme, deep mesencephalic nucleus; DTT, dithiothreitol; EAE, experimental autoimmune encephalomyelitis; ec, external capsule; epl, external plexiform layer of the olfactory bulb; fr, fasciculus retroflexus; fmi, forceps minor of the corpus callosum; gcc, genu of the corpus callosum; ic, internal capsule; IMS, imaging mass spectrometry; ipn, interpeduncular nucleus; lgn, lateral geniculate nucleus; lo, lateral olfactory tract; MALDI, matrix-assisted laser desorption/ionization; MBP, myelin basic protein; MS, mass spectrometry; MW, molecular weight; opt, optic tract; pag, periaquaductal gray; pn, pontine nuclei; ROI, region of interest; sc, superior colliculus; sn, substantia nigra; TBS, Tris buffered saline; TFA, trifluoroacetic acid; THAP, 2,4,6-trihydroxyacetophenone; TOF, time-of-flight; vp, ventral posterior thalamic nucleus; zi, zona incerta

* Corresponding author. Tel.: +32 16 323926; fax: +32 16 324263.
E-mail addresses: Ruben.ceuppens@bio.kuleuven.be (R. Ceuppens), Debora.Dumont@uhasselt.be (D. Dumont), Leen.vanbrussel@bio.kuleuven.be (L. Van Brussel), Babs.vandeplas@bio.kuleuven.be (B. Van de Plas), Ruth.Daniels@uhasselt.be (R. Daniels), JeanPaul.Noben@uhasselt.be (J.-P. Noben), Peter.Verhaert@udelft.nl (P. Verhaert), Estel.vandergucht@bio.kuleuven.be (E. Van der Gucht), Johan.Robben@uhasselt.be (J. Robben), Stefan.clerens@canesis.com (S. Clerens), Lut.arckens@bio.kuleuven.be (L. Arckens).
[1] Both authors contributed equally to this paper.
[2] Present address: Protein Science and Structural Biology, Canesis Network Ltd., Private Bag 4749, Christchurch, New Zealand. Tel.: +64 3 325 6641; fax: +64 3 325 2717.

1387-3806/$ – see front matter © 2006 Elsevier B.V. All rights reserved.
doi:10.1016/j.ijms.2006.09.007

1. Introduction

In the past decade, proteomics has become an indispensable tool in biomedical research, traditionally combining high-resolution separation techniques and highly sensitive detection methods. Due to its high sensitivity and specificity, mass spectrometry (MS) became the method of choice for the analysis of proteins and peptides [1]. Techniques such as matrix-assisted laser desorption/ionization mass spectrometry (MALDI MS) [2,3] and significant improvements of time-of-flight mass spectrometers [4,5] have revolutionized the ability to analyze proteins. The combination of MALDI MS with a separation technology such as two-dimensional gel electrophoresis or liquid chromatography has therefore been recognized as ideal tools to investigate complex protein mixtures [6–8]. However, in this type of analyses, proteins are extracted from tissues and information regarding the spatial localisation of a given protein clearly is lost.

Imaging mass spectrometry (IMS) is a new technology that utilizes various MS techniques for the simultaneous mapping of hundreds of peptides and proteins present in thin tissue sections [9]. Subsequently, specific information on the relative abundance and spatial distribution of proteins can be obtained, providing the opportunity to correlate ion images with histological features observed by light microscopy. IMS represents an excellent discovery tool in research since the proteins recorded do not need to be known in advance and no label or reporter system is required to generate the protein specific images [13]. Protein profiling by IMS has been performed on human brain tumour xenografts [10], rat pituitary [11], mouse brain [10], mouse prostate [12], mouse epididymis [13] and in animal models for neurological disorders, including Parkinson's [14] and Alzheimer's disease [15]. Mass spectral patterns from tissue sections of brain [16,17] and lung tumours [18] identified protein patterns that not only correlate with tumour histology but also with patient survival. Nevertheless, unknown compounds can be identified via retrospective analysis of the data obtained from an experiment [19]. This was demonstrated for some of the differentially expressed proteins in the cancer studies described above. These examples illustrate how the integration of IMS into protocols for disease diagnostics as well as outcome prediction might soon take place [20]. IMS can also be applied to detect pharmaceutical compounds in tissues, as shown for the antipsychotic drug clozapine in rat [21]. In this context, the potential capability of IMS to assess adequacy of delivery of chemotherapeutic agents to a particular organ site is a particularly exciting application of this technology [22,23]. In conclusion, IMS can provide unique information and is believed to greatly facilitate our molecular understanding of normal and pathological processes [24].

Very recently, it was shown that myelin basic protein could be visualized in white matter structures like the corpus callosum in mouse brain using IMS [25]. Because of the devastating role of myelin loss in a number of central nervous system disorders, most notably multiple sclerosis, we designed this study to investigate whether MALDI IMS as developed in our laboratories is sensitive enough to analyze the distribution of different MBP isoforms and to visualize and localize focal regions of experimentally induced demyelination in mouse brain.

2. Experimental/material and methods

2.1. Animals and tissue preparation

All experiments were conducted according to the European Communities Council Directive of 24 November 1986 (86/609/EEC), and carried out in accordance with institutional animal welfare guidelines (K.U. Leuven, Leuven, Belgium). These rules were followed strictly in all experiments. All efforts were made to minimize the animals' discomfort and to reduce the number of animals.

All experiments have been performed on adult C57Bl/6 mice (Janvier).

Six animals were killed by cervical dislocation, the brains were rapidly removed and immediately frozen in liquid nitrogen cooled isopentane and stored at −70 °C until sectioning in order to minimize protein degradation caused by temperature and oxidation [26]. The tissue was applied in MBP extraction ($n = 1$) or IMS ($n = 5$).

Two animals were sacrificed with an overdose of sodium pentobarbital (60 mg/kg, i.p.) and were immediately perfused transcardially with 0.9% saline, followed by cold 4% paraformaldehyde (Sigma–Aldrich, St. Louis, MO) in 0.15 M sodium phosphate buffer (PBS, pH 7.4). Brains were removed from the skull, postfixed, rinsed, and stored at 4 °C in PBS containing 0.01% sodium azide until processed for MBP immunohistochemistry.

2.2. MBP extraction

The MBP extraction procedure was adapted from the procedure described by Maatta et al. [27]. Briefly, one whole frozen mouse brain was homogenized in 5 ml chloroform with an Ultra-Turrax (type TP18/10; IKA, Janke and Kunkel, Staufen, Germany). Following centrifugation at $4500 \times g$ for 5 min, the chloroform fraction was collected and the aqueous phase was discarded. The tissue was re-extracted with 2.5 ml chloroform and the chloroform fraction was separated as described above. The pooled chloroform fraction was washed with 4.5 ml water, followed by the addition of 3 ml methanol to the separated chloroform fraction. To this mixture 1.5 ml water containing 40 μl of 1 M HCl was added. At pH 2.0, the acidic aqueous phase was separated from the chloroform fraction as described above. In total, 3 ml of aqueous phase was collected and taken to dryness by in vacuo centrifugal evaporation. The residue was dissolved in 200 μl of a 0.1% TFA solution in water.

2.3. Tryptic digestion of MBP

To a 10 μl aliquot of isolated MBP, 75 μl 50 mM NH_4HCO_3 and 2 μl reducing agent (45 mM DTT in 50 mM NH_4HCO_3) were added. The sample was incubated at 56 °C for 15 min followed by the addition of 2 μl alkylating solution (100 mM

iodoacetamide in 50 mM NH_4HCO_3) and incubation at room temperature for 15 min. The mixture was subjected to trypsin digestion (Promega, Leiden, The Netherlands; enzyme:protein ratio 1:50, 37 °C, overnight). The reaction was stopped by adding 5 μl of a 10% TFA solution and the digested protein sample was taken to dryness by in vacuo centrifugal evaporation.

2.4. Matrix-assisted laser desorption/ionization (MALDI) mass spectrometry of MBP

A sample of MBP extract (2 μl) was mixed with 2 μl of TFA 2.5% and 2 μl of THAP matrix (2,4,6-trihydroxyacetophenone; 7.6 mg/ml in EtOH/water, 3/1, v/v) followed by spotting of 1 μl on a MALDI target plate (anchorchip 600 μm, Bruker, Bremen, Germany) for precise protein MW determinations. The molecular masses present in the MBP extract were determined using a MALDI TOF-TOF Instrument (Ultraflex II, Bruker) equipped with a SmartBeam laser and operated under *FlexControl*. Spectra were calibrated in FlexAnalysis using the Protein Calibration Standard I (Bruker).

A sample of the MBP tryptic digest (1 μl) was spotted on a MALDI target plate (anchorchip 600 μm, Bruker) and allowed to dry after which 0.5 μl of CHCA matrix (final concentration 0.66 mg/ml in ACN/2.5% TFA, 2/1, v/v) containing THAP (final concentration 1 mg/ml in ACN/2.5% TFA, 2/1, v/v) was added. Following peptide mass fingerprinting and MALDI TOF-TOF analysis, spectra were calibrated in FlexAnalysis using the Peptide Calibration Standard I (Bruker). Data files were searched with Mascot (Matrix Science, London, UK) using the NCBI database.

2.5. MBP immunohistochemistry

Brains of two adult mice were used. Coronal sections (50 μm) were cut on a vibratome and collected in serial order. Series of free-floating sections were processed for immunohistochemistry or were Nissl stained with cresyl violet (1%) (Fluka Chemical, Sigma–Aldrich) following standard procedures.

Endogenous peroxidase activity was first blocked with 0.3% H_2O_2 for 20 min. Then the free-floating sections were pre-incubated with normal goat serum (NGS, 1/10, 45 min), followed by an overnight incubation with the rat primary antibody against MBP (RDI-MBPabrt-12, Research Diagnostics Inc., Concord, USA) at a 1/100 dilution. The antibody is raised against an epitope shared by all MBP mouse isoforms ($n = 13$) except isoform 2 (GolliMBP2) and isoform 3 (GolliMBP3). For detection, biotinylated rabbit anti-rat IgGs (1/400; 30 min; Dako, Glostrup, Denmark) in combination with peroxidase-conjugated Streptavidin (1/500; 30 min; Dako) were applied. The reaction product was visualized as a black precipitate using the glucose oxidase-DAB-nickel method [28]. All incubations and rinses were performed at room temperature under gentle agitation in Tris buffered saline (TBS, 0.01 M Tris, 0.9% NaCl, 0.3% Triton-X 100, pH 7.6). Sections were mounted on gelatin-coated slides, dehydrated, cleared, coverslipped and viewed under a Leitz DM RBE microscope (Leica, Leitz Instruments, Heidelberg, Germany).

2.6. Ethidium bromide injection

Twelve-week-old male mice ($n = 2$) were anaesthetized with Ketalar/Domitor (i.p., 0.3 ml/0.2 ml mixture, 50 mg/ml ketamine hydrochloride, 1 mg/ml Domitor; Pfizer) at a dose of 8 μl/g body weight. After application of xylocaine ointment (5%, AstraZeneca) a small incision was made on the scalp to expose the skull and drill two small holes. A micropipette attached to a Hamilton syringe was used for the delivery of 1 μl of 0.1% ethidium bromide using the following stereotactic coordinates according to the atlas of Franklin and Paxinos [29]: 1.8 mm from the midline (right or left), 1.7 mm anterior from bregma and depth 2.5 mm. The skin was sutured. The animals were allowed to recover on a heated pad after injection with Antisedan (0.5 mg/ml, 15 μl/g bodyweight, i.m., Pfizer) and were kept for 2 weeks.

Brains of the ethidium bromide injected mice ($n = 2$) and of normal control animals ($n = 3$) were sectioned coronally on a cryostat (Microm, Waldorf, Germany) at −16 °C. Ten micrometer sections for IMS were placed on a MALDI target plate using forceps. Adjacent sections (10 or 50 μm) for routine histology were mounted on 0.1% poly-L-lysine (Sigma–Aldrich) coated slides and were stained with thionine following standard procedures. These thionine-stained sections were used to correlate the IMS signals with specific brain regions as well as to check correctness of the ethidium bromide injection sites [29].

Intensity differences (peak height differences) in MBP expression inside and outside the injection site were quantified. In each animal ($n = 2$), data from the left and/or right hemisphere were collected. The ROI had an average size of 56 and 145 pixels (that is 0.56–1.45 mm^2 based on a 100 μm pixel resolution), respectively, in the demyelinated regions and the surrounding white matter. IMS images and adjacent thionine-stained sections were compared to determine the position of the injection site and the reference area. Data are presented as percent decrease with the value in normal unlesioned white matter set at 100%.

2.7. MALDI IMS (see workflow in Fig. 1) (for details on software see Ref. [31])

Tissue sections collected on the MALDI target plate were lyophilised for a minimum of 1 h (Fig. 1). The dry sections were subsequently fixed/washed by covering the MALDI target plate with 30:70 H_2O:ethanol (VWR International, France) for 30 s, drying for 1 min, covering with 5:95 H_2O:ethanol solution and drying.

The sections were spray-coated with matrix using a simple nebulizer. The nebulizer consisted of a coaxially joined flow (100 μl/min) of matrix solution and N_2 gas (1.5 bar), mounted on a flatbed *XY* plotter (Graphtec 2000). The matrix solution was 10 mg/ml sinapinic acid (Fluka-Sigma, Bornem, Belgium) in 50% acetonitrile (HPLC-grade, Riedel-deHaën, Hannover, Germany) in HPLC-grade water (Riedel-deHaën) with 0.1% trifluoroacetic acid (99%, Acros Organics, Geel, Belgium). Prior to spray-coating, the tissue sections were covered with fine sinapinic acid seed crystals [31,32].

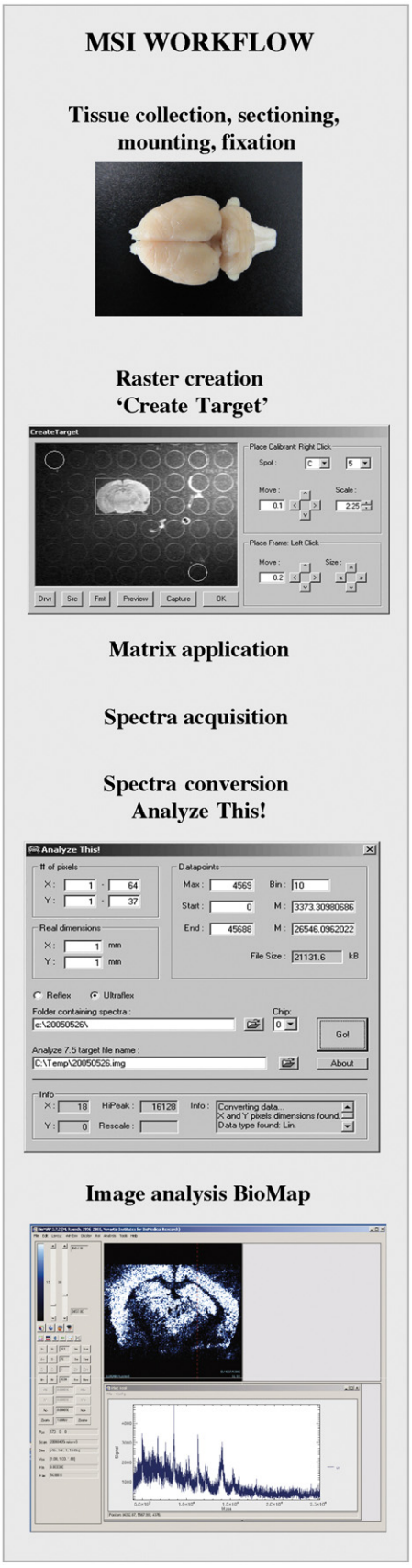

An in-house developed program, *CreateTarget* (copyright S. Clerens), was used to create a geometry file describing a raster of sample points according to the dimensions of the tissue section. This file was imported in the *FlexControl* software that controls the Ultraflex II mass spectrometer (Bruker). This allowed the automated acquisition of spectra according to the defined grid. Coronal tissue sections of 10 μm were analyzed using a 50 μm step size in the *XY* plane. Spectra were calibrated using the singly and doubly charged ions of haemoglobin alpha and beta as previously described by Chaurand and Caprioli [33].

For image processing the *BioMap* software was used (http://www.maldi-msi.org). To allow import of the array of spectra in *BioMap*, the spectra had to be converted to the Analyze 7.5 format. For this purpose we developed a program (*Analyze This*!, copyright S. Clerens), which reads all binary format spectra acquired in an IMS experiment and stores the data in a single Analyze 7.5 file.

3. Results

A first set of experiments identified different ion peaks, within a spectrum of a mass range from 5000 to 25,000 Da, showing a typical distribution pattern consistent with white matter structures in coronal sections of mouse forebrain. As illustrated in Fig. 2, ions of *m*/*z* 14,144 and 18,447 indeed displayed a density map that specifically resembled white matter patterns in mouse brain. In view of the great interest in the molecular mechanisms of myelin disorders like multiple sclerosis (an autoimmune inflammatory demyelinating disease of the central nervous system) we initiated an in depth study of these two ions which could reveal relevant data with respect to our molecular understanding of these types of pathologies.

The proteins at *m*/*z* 14,144 and 18,447 could indeed be important myelin components namely myelin basic protein isoform 8 (MBP-8) and isoform 5 (MBP-5; theoretical mass, respectively, 14,211 and 18,488 Da). To confirm this we employed the procedure of Maatta et al. [27] to isolate MBP from whole mouse brain by means of chloroform extraction for MS analysis (Fig. 3). Direct MALDI TOF analysis of the tissue extract in linear mode (*m*/*z* 4,000–30,000) resulted in two major signals detected at *m*/*z* 14,139 and 18,416. These masses correspond, respectively, to isoform 8 and 5 of mouse MBP (SWISS-PROT accession number P04370-8 and -5) described in literature as the most abundant MBP isoforms in mouse brain [27]. The experimental masses observed in this study can be related to the theoretical mass as illustrated in Table 1, leaving only 3 Da unaccounted for, which might be due to additional citrullination or calibration error. These masses are in correspondence with a previous MS study on MBP [34]. In addition, signals detected

Fig. 1. Our MALDI IMS workflow indicating the necessary steps between tissue collection and imaging the distribution of an ion with a specific *m*/*z* value in a tissue section: tissue collection, sectioning and mounting of sections on the MALDI target plate, fixation, creating a raster using *Create Target* freeware, matrix application using a home-built nebulizer, spectrum acquisition on an Ultraflex II Instrument using *FlexControl*, spectrum conversion into an image using *Analyze This*! and *BioMap*.

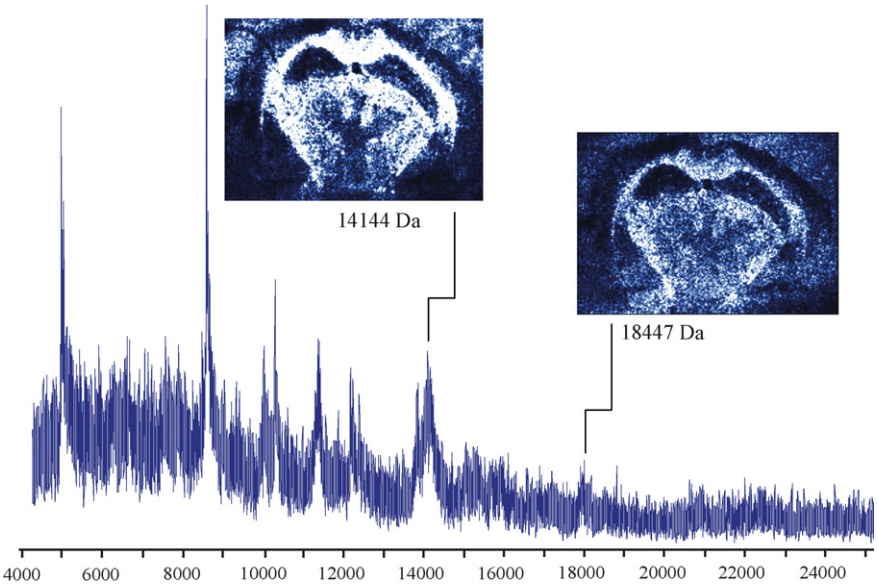

Fig. 2. MALDI IMS allows for simultaneous differential mapping of several ions. A mass spectrum (baseline-corrected) acquired from one position on a 10 μm mouse brain cryostat section and the corresponding distribution pattern for two ions, *m/z* 14,144 and 18,447, with a clearly white matter-related distribution pattern in mouse brain, as extracted from the spectra of all data points assessed throughout the whole section.

at *m/z* 7068/9211 Da and at 4710/6135 represent the doubly and triply charged ions of the MBP-8 and MBP-5 isoforms, respectively. Table 1 summarizes the mass determination of differently charged MBP ions, including parameters for resolution and full width at half maximum (FWHM). Peptide mass fingerprinting (in reflectron mode, Fig. 3A) resulted in an MBP (isoform 5) sequence coverage of 69%. MALDI TOF-TOF analysis on two selected precursor ions unambiguously confirmed the identity of MBP-5 and MBP-8 (Fig. 3B and C).

Immunohistochemistry for MBP further showed a great overlap in the distribution of MBP as detected with MBP specific antibodies in comparison to the MBP-5 (Fig. 4A) and MBP-8 (Fig. 4B) patterns generated with MALDI IMS. Evaluation of the different MBP expression profiles revealed how MALDI IMS leads to a better visualization of intensity differences for the MBP isoforms over different white matter regions. The relative quantitative character and the isoform specificity of the IMS data are two advantages with respect to the more commonly applied immunohistochemical detection method.

To assess the ability of IMS to detect changes in MBP expression under different pathological conditions, we elicited a focal demyelination of the corpus callosum by injection of a gliotoxic agent. A localized lesion was induced in the forceps minor of the corpus callosum (fmi) of 12-week-old mice using the ethidium bromide injection paradigm [30,35]. As illustrated in Fig. 5, MALDI IMS of the ion with *m/z* 14,144, MBP-8, visualized the experimentally induced condition of demyelination. A thionine-stained section (Fig. 5A) illustrates the position of one needle track and the two injection sites, exactly positioned inside the left and right forceps minor of the corpus callosum. The IMS image of the adjacent section (Fig. 5B) demonstrates a clear MBP-8 intensity loss at the exact same locations within the fmi. When the signal intensity in a region of interest (ROI) placed within this location was compared to a ROI in the intact fmi, a

Table 1
Mass spectrometric mass determination of MBP

Component	$Mass_{theor}$[a] (Da)	Suggested PTM[b] (Da)	$Mass_{cal}$[c] (Da)	$Mass_{obs}$[d] (Da)	ΔMass (Da)	ΔMass (%)	FWHM[e]	Res[f]
[MBP-8 + H^+]	14,211	−Methionine (131) + acetyl (42) + methyl (14)	14,136	14,139	3	0.02	64.3	220
[MBP-8 + $2H^+$]			7,069	7,068	1	0.01	41.7	169
[MBP-8 + $3H^+$]			4,713	4,710	3	0.06	24.3	194
[MBP-5 + H^+]	18,488	−Methionine (131) + acetyl (42) + methyl (14)	18,413	18,416	3	0.02	61.3	301
[MBP-5 + $2H^+$]			9,207	9,211	4	0.04	46.4	198
[MBP-5 + $3H^+$]			6,138	6,135	3	0.05	23.9	257

[a] Theoretical mass derived from Swiss-Prot (P04370-8 and P04370-5).
[b] Suggested posttranslational modifications (PTM) of MBP.
[c] Calculated mass.
[d] Observed mass.
[e] Full width at half maximum of recorded masses.
[f] Resolution of recorded masses.

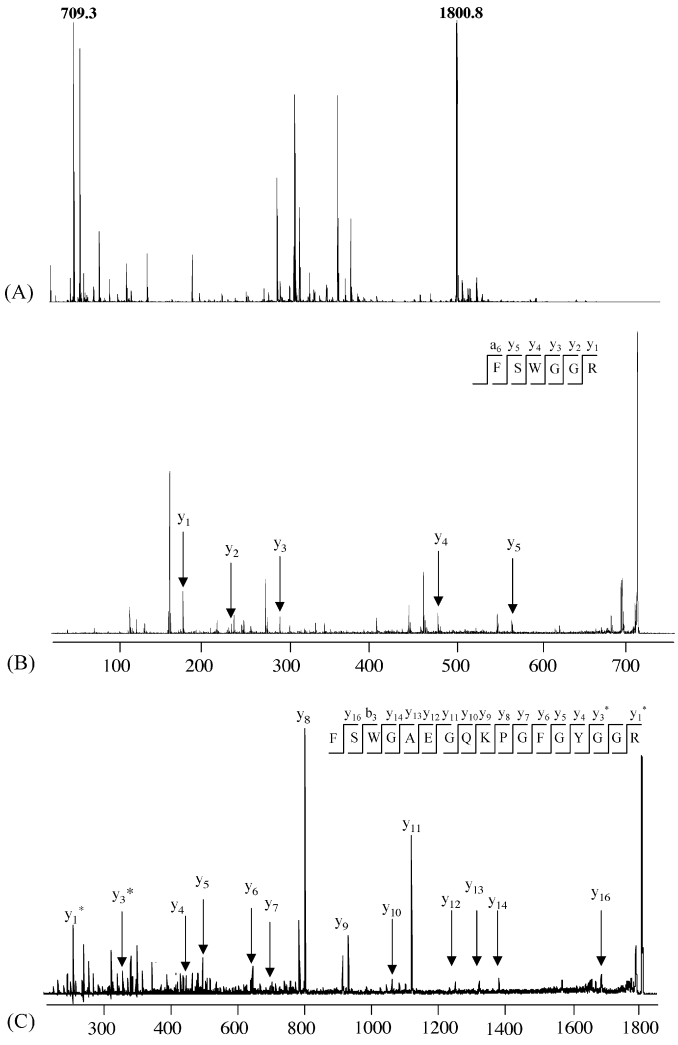

Fig. 3. Identification of ions of *m/z* 14,144 and 18,447 as MBP isoform 8 and 5. MBP was isolated from mouse brain by chloroform extraction. The tissue extract was digested and subjected to peptide mass fingerprinting (A). MALDI-MS/MS analysis of the precursor ions of *m/z* 709.3 and 1800.8 followed by database searching unambiguously identified the ions as MBP-5 (B) and MBP-8 (C).

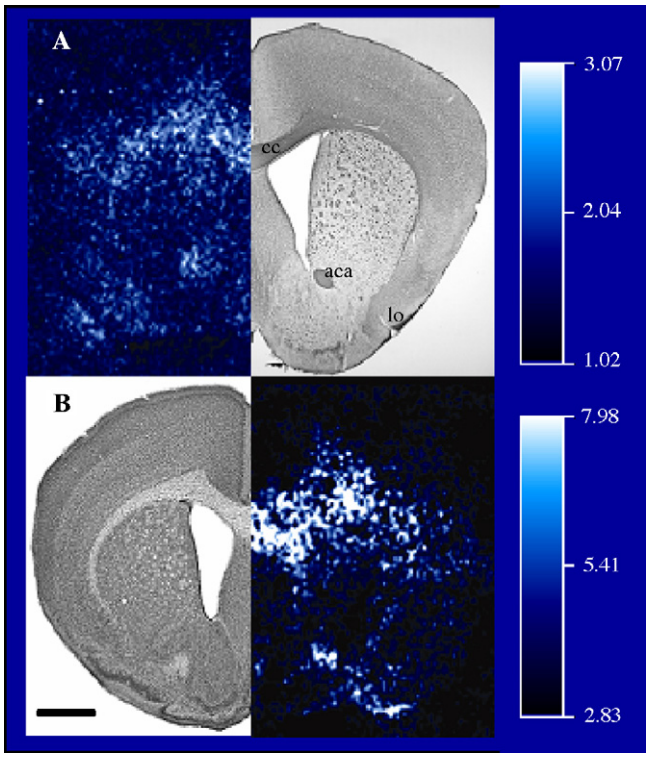

Fig. 4. Comparative analysis of MBP distribution by MALDI IMS and immunohistochemistry. Comparison of the *m/z* 18,447 image (A, left side), the *m/z* 14,144 image (B, right side), the photograph of a similar section immunostained for MBP (A, right side) and a similar section counterstained with cresyl violet (B, left side) illustrates the detection of these ions in typical white matter structures of the brain: anterior commissure, corpus callosum, lateral olfactory tract (aca, cc, lo). Note that immunohistochemistry also detects additional MBP isoforms in other brain regions like the neocortex. Scale bar: 1 mm; intensity scale: value × E+05.

clear intensity loss of 40% could be shown for MBP-8 (Fig. 5C). The same trend, although to a lesser extent, was observed for the MBP-5 signal. Other myelinated structures that were easily recognized when comparing the thionine-stained section with the adjacent MBP IMS images are the anterior part of the anterior commissure (aca) and the lateral olfactory tract (lo) at the extreme left and right outer borders of the deep part in the mouse brain.

A final set of experiments was designed to map the distribution of MBP-8 along the anterior–posterior axis of the mouse brain. We selected coronal sections to include levels between bregma 2.68 and −3.80 in which typical white matter structures and brain regions rich in passing axon bundles are located, some of which can be recognized at various anterior to posterior locations (Fig. 6). We here describe the various brain structures that showed a significant expression of ion 14,144, MBP-8, starting from the most anterior coronal plane that was analyzed.

Imaging mass spectrometry of ion 14,144 resulted in the visualization of the external plexiform layer (epl) of the olfactory bulb and the lateral olfactory tract (lo) at far anterior levels in the mouse brain, such as 2.68 mm from bregma (Fig. 6A). At bregma 0.98 (Fig. 6B), the profile of the genu of the corpus callosum (gcc) was clearly visible, connecting the two hemispheres and contacting the more dorsal cingulum (cg) and the more lateral external capsule (ec). More ventrally in this same section, a clearly delineated circular anterior commissure (aca) as well as the lateral olfactory tract could be distinguished. At bregma −1.46 (Fig. 6C), the dorsal horn of the hippocampus (dhc) was clearly outlined as an MBP-negative structure by surrounding myelin-rich structures, dorsally the corpus callosum and the cingulum and ventrolaterally the hippocampal fimbria (fi). Below the fimbria, the internal capsule (ic) and the ventral posterior thalamic nucleus (vp) were intensely outlined. Next, a more posterior brain section (bregma −2.46; Fig. 6D) illustrates the corpus callosum bridging the two hemispheres and forming a continuum dorsally with the cingulum and ventrolaterally with the external capsule. Below the dorsal horn of the hippocampus, the lateral geniculate nucleus (lgn) complex was also found myelin rich. As for the ventral posterior thalamic nucleus in panel C, this is consistent with the high number of afferent and efferent axonal connections this thalamic nucleus

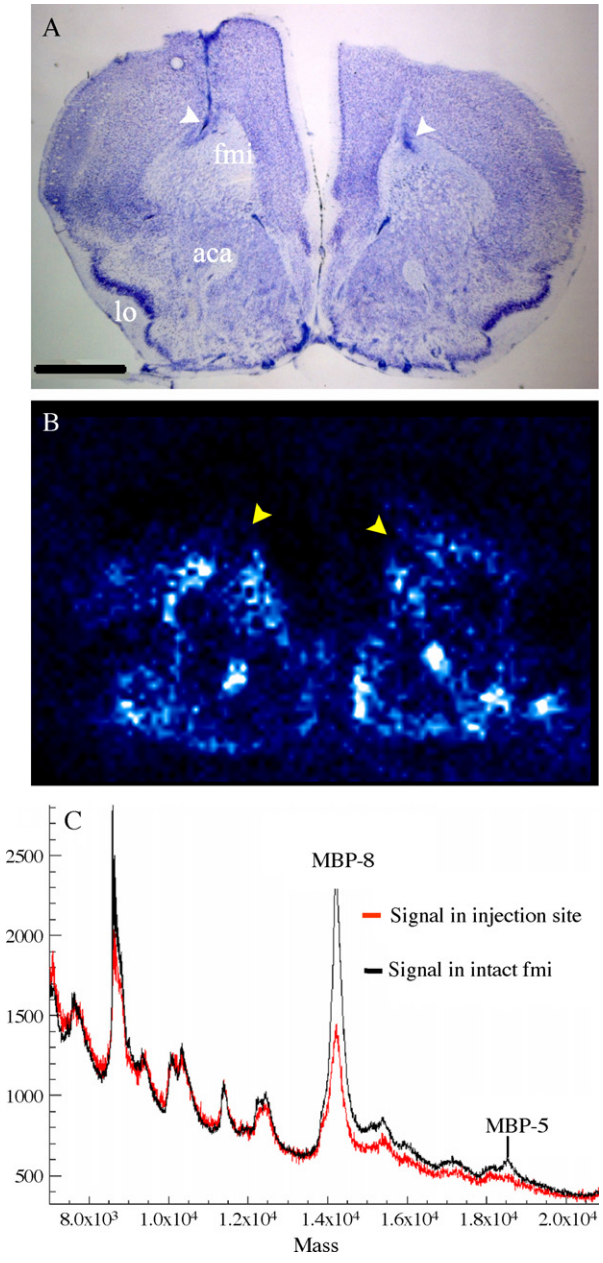

Fig. 5. Effect of ethidium bromide injections on the detection of *m/z* 14,144. Local injection of ethidium bromide into the fmi (forceps minor of the corpus callosum), a typical white matter structure of the forebrain (panel A), clearly resulted in an intensity loss for the ions of *m/z* 14,144 (B). The dimensions and position of the ethidium bromide effect matched the injection site as detected by thionine staining of an adjacent brain section (A). The ethidium bromide-invoked demyelination thus nicely correlated to the loss in signal intensity for MBP-8 and MBP-5 in the affected region compared to the intact fmi (C). Scale bar: 1 mm.

has as a relay station for sensory information to sensory cortex. Below the lgn, the optic tract (opt) and the cerebral peduncle (ce), and more medially also the zona incerta (zi) displayed high MBP-8 levels. Immediately adjacent to the midline the fasciculus retroflexus (fr) stood out as a heavily myelinated axon bundle.

At bregma level −3.8 (Fig. 6E), the corpus callosum and the external capsule form a thin white matter sheath underlying the different neocortical areas. In the midbrain, the periaqueductal gray (pag), the substantia nigra (sn) and the interpeduncular nucleus (ipn) contrasted as myelin poor regions compared to the deep mesencephalic nucleus (dpme) and the pontine nuclei (pn). Dorsal to the pag, the superior colliculus (sc) showed moderate levels of MBP-8.

4. Discussion

Multiple sclerosis is believed to result from an autoimmune reaction against myelin components of the central nervous system. The demyelination process is characterized by an inter-individual but not intra-individual heterogeneity, and four distinct (but overlapping) patterns of focal demyelination were identified histologically in biopsy and autopsy material [36,37]. Nevertheless, disease mechanisms in multiple sclerosis remain poorly understood at the molecular level and no reliable proteinaceous disease markers are available yet. Although animal models for multiple sclerosis are extensively used to study etiology, pathogenesis and new therapeutic approaches, only a limited number of proteomic studies have been published so far [38]. Since IMS was previously shown to be a valuable tool in the investigation of other neurological disorders [14,15], we initiated a MALDI IMS approach to perform an assessment of protein patterns in different areas of mouse brain and to illustrate the potential of MALDI IMS to study demyelination in a mouse model as a pathological disease mechanism. This study illustrates the detection of two isoforms of myelin basic protein (MBP) using a combination of high-resolution MALDI IMS, MBP-immunohistochemistry and mass spectrometric analysis of isolated MBP. Furthermore, upon ethidium bromide injection in the corpus callosum, a marked and localized reduction of the MBP protein peaks was demonstrated, indicative for demyelinated lesions. This study therefore undeniably demonstrates the potential of MALDI IMS to study myelination and demyelination processes in different neurological disorders including multiple sclerosis.

Our research showed that in IMS experiments, MBP is highly susceptible to protein delocalisation due to diffusion. Utmost care was taken to achieve good extraction of proteins out of the tissue, but to limit their delocalisation. The nature of MBP however is such that a minimal delocalisation cannot be avoided (Fig. 6D, upper right corner). Matrix-coating with a nebulizer is always a compromise between maximizing the extraction of proteins and minimizing the delocalisation of these same proteins. The use of an automated nebulizer allowed the application of a homogeneous matrix-coating on the total tissue section surface in a reproducible manner, so MBP imaging with a high-resolution raster of sample points was possible. Calibration of the IMS spectra using the singly and doubly charged hemoglobin-alpha and -beta chains as described by Chaurand and Caprioli [33] resulted in *m/z* 14,144 for MBP-8 and *m/z* 18,416 for MBP-5. It was not unexpected that the masses observed for MBP spotted directly on target and MBP in tissue sections deviated (0.042 and 0.16% for MBP-8 and MBP-5, respectively). MALDI analysis of samples located at different places on a MALDI target plate can generate differ-

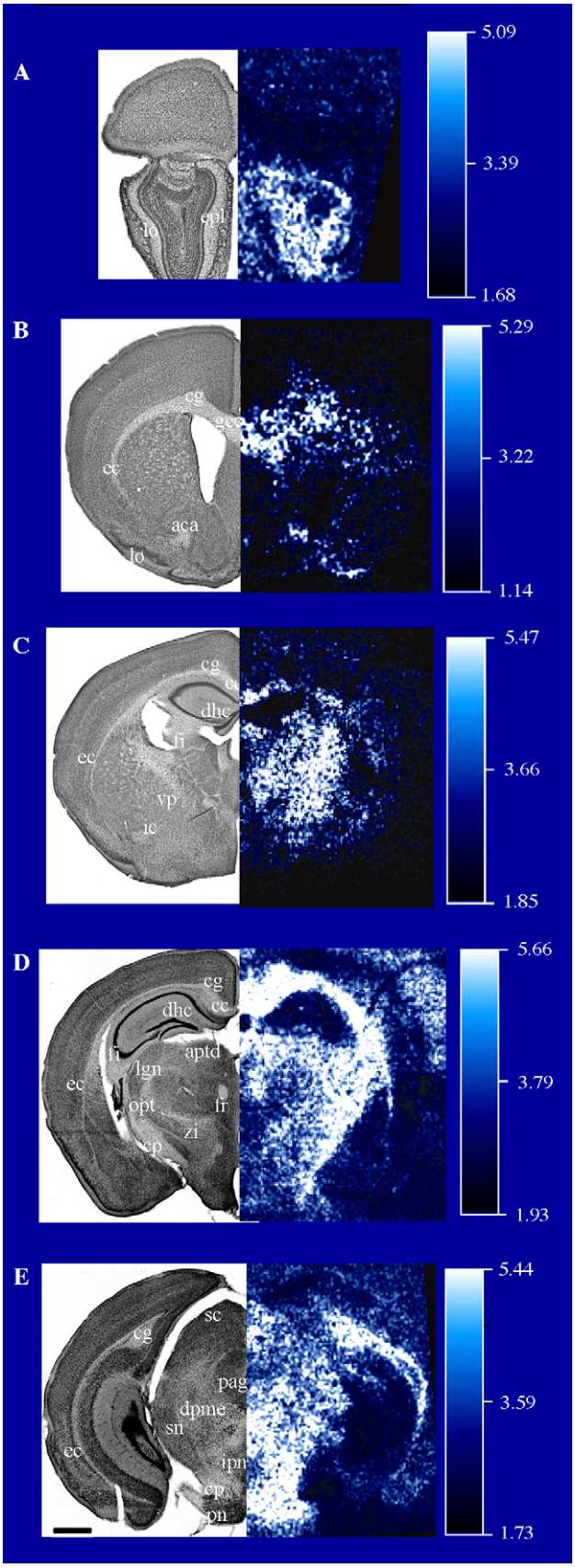

ent masses. Therefore, frequent calibration is necessary. Since hemoglobin peaks are present mainly at the border of the tissue slice, adequate calibration for all locations in tissue sections is often impossible.

Experimentally induced demyelination due to direct injection of gliotoxic agents has provided powerful models for studying the biology of de- and remyelination. For the most part these models have involved injection of gliotoxins like ethidium bromide in white matter of the central nervous system, producing localized areas of demyelination with minimal axonal damage [29]. Here, the purpose of the ethidium bromide injection was to deliver proof of principle that MALDI IMS can detect circumscribed changes in isoform specific MBP expression at a given location in mouse brain. Therefore, we sacrificed mice at 14 days post injection, a time point at which lesions remained demyelinated with little or no evidence of remyelination [30]. Analysis of the signal intensity of the MALDI IMS data showed a 40% reduction of the MBP-8 ion density at the ethidium bromide delivery site as compared to the surrounding unaffected white matter. According to a study in rats by Franklin and Woodruff [30], ethidium bromide injections can cause lesions ranging in size from 0.25 to 1.75 mm^2, depending on the ethidium bromide volume and concentration. In our study, the size of the lesion at day 14-post injection is estimated to be 0.4–0.6 mm^2 as evidenced by thionine staining and the MS images (Fig. 4), in full agreement with observations in mouse by Liu et al. [35].

Altogether our observations not only open new perspectives for applying MALDI IMS in future experiments concerning demyelination but also for assessing the occurrence of remyelination based on MBP expression profiles by analyzing 6–14 week post injection survival times [30]. Hence, we illustrated that MALDI IMS is capable of detecting localized changes in protein expression and can subsequently be applied to study biological and pathological processes. With respect to multiple sclerosis, these processes do not only include de- and remyelination but also inflammation. The aspect of inflammation might be studied by comparing protein profiles from healthy subjects with those from gliotoxic lesions and from the models of experimental autoimmune encephalomyelitis (EAE). Brain stem sections of EAE rats stained with an antibody directed against CD68,

Fig. 6. Ion density maps for the signal at *m/z* 14,144 along the anterior posterior axis of the mouse brain. The ion density maps were recorded with a spatial resolution of 50 μm. The different frontal planes were chosen along the anterior posterior axis of the brain as to sample different white matter structures. Five pairs of MALDI IMS images and photographs of cresyl violet stained sections are shown to identify and indicate the different brain structures that show a high intensity for the MBP-8 ion. The highest signals were detected in typical white matter structures and brain regions rich in passing fibres like the cc, lo, fr, cg, ce and aca. *Abbreviations:* aca: anterior commissure, aci: intrabulbar anterior commissure, aptd: dorsal part of the anterior pretectal nucleus, cc: corpus callosum, cg: cingulum, cp: cerebral peduncle, dhc: dorsal horm of the hippocampus, dpme: deep mesencephalic nucleus, ec: external capsule, epl: external plexiform layer of the olfactory bulb, fi: fimbria of the hippocampus, fr: fasciculus retroflexus, gcc: genu of the corpus callosum, ic: internal capsule, ipn: interpeduncular nucleus, lgn: lateral geniculate nucleus, lo: lateral olfactory tract, opt: optic tract, pag: periaquaductal gray, pn: pontine nuclei, sc: superior colliculus, sn: substantia nigra, vp: ventral posterior thalamic nucleus, zi: zona incerta. Scale bar: (A) 500 μm, (B–E) 750 μm; intensity scale: value × E+05.

a marker for monocytes, displayed multiple infiltration sites of 0.4–0.6 mm^2, hence situated within the MALDI IMS study window (unpublished observation). The identification of specific patterns of myelin-related proteins in a single analysis clearly offers unique possibilities for such comparative studies. In addition, MALDI IMS may be applied to study the delivery and distribution of therapeutic agents in brain tissue of different animal models for diverse white matter disorders.

Comparison of the MBP MALDI IMS data with the immunohistochemical MBP expression profile further illustrated the complementary character of MALDI IMS to other protein imaging methods. Indeed, whereas immunohistochemistry creates spatial distribution profiles with cellular resolution, the method has only limited quantitative power and visualizes several MBP isoforms together due to the present lack of commercially available isoform-specific antibodies. In contrast, MALDI IMS technology categorically allowed the separate visualization of two MBP isoforms with differences in ion intensity as a quantitative measure. Yet quantitative interpretation of IMS signals has also to be carried out with caution because true peak intensity differences might be influenced by ionization efficacy, ion suppression and the absence or presence of posttranslational modifications in the protein under study. This is particularly important when looking at a protein like MBP, a member of a larger family of proteins with a multiplicity of forms and posttranslational modifications, including phosphorylation, deamidation, citrullination and methylation [39]. Also low abundant isoforms or regions of low expression may remain undetected because of limited protein extraction efficiency or the instrument sensitivity threshold.

Different imaging modalities are often combined in neuroimaging to assist in the understanding of brain functions in normal and diseased stages. Although positron emission tomography and functional magnetic resonance imaging are excellent tools to gather anatomical, physiological and functional information about the brain, none of these methods have the ability to visualize protein distribution patterns. On the other hand, the combined use of immunohistochemistry and MALDI IMS holds great promise in future investigations to allow two- and even three-dimensional representation of proteins in their full spatial and multi-dimensional distribution in different tissues under normal and pathological conditions [25].

5. Conclusion

MALDI IMS creates an excellent opportunity to correlate ion images with anatomical and histochemical features and allows for the simultaneous mapping of several proteins in a certain tissue section within one experiment, without the need for ultra-specific antibodies. We clearly illustrated the power of MALDI IMS to study both normal and abnormal white matter regions in brain. Correlating changes to local protein distributions caused by diseases such as multiple sclerosis will help in providing a more complete understanding of such myelin disorders. An important prospect for our MALDI IMS experiments lies in future evaluations of the potential of IMS analysis of postmortem brain slices of multiple sclerosis patients which may lead to the identification of proteins that will allow subtyping and, in due time, development of personalized therapies for multiple sclerosis patients. In this respect, a major challenge remains the identification of ions of interest directly from the tissue upon imaging.

Acknowledgments

We are grateful to Lieve Geenen, Ria Vanlaer and Erik Royackers for expert technical assistance. This work was supported by the F.W.O. Flanders, the Research Council of the K.U. Leuven (0T 05/33) and the Belgian WOMS (Wetenschappelijk Onderzoek Multiple Sclerosis) Foundation.

References

[1] T.C. Rohner, D. Staab, M. Stoeckli, Mech. Ageing Dev. 126 (2005) 177.
[2] F. Hillenkamp, M. Karas, R.C. Beavis, B.T. Chait, Anal. Chem. 63 (1991) 1193A.
[3] M. Karas, M. Gluckmann, J. Schafer, J. Mass Spectrom. 35 (2000) 1.
[4] R.S. Brown, J.J. Lennon, Anal. Chem. 67 (1995) 1998.
[5] M.L. Vestal, J.M. Campbell, Methods Enzymol. 402 (2005) 79.
[6] P. Roepstorff, Curr. Opin. Biotechnol. 8 (1977) 6.
[7] R. Aebersold, D.R. Goodlett, Chem. Rev. 101 (2001) 269.
[8] A. Pandey, M. Mann, Nature 405 (2000) 837.
[9] P. Chaurand, S.A. Schwartz, M.L. Reyzer, R.M. Caprioli, Toxicol. Pathol. 33 (2005) 92.
[10] M. Stoeckli, P. Chaurand, D.E. Hallahan, R.M. Caprioli, Nat. Med. 7 (2001) 493.
[11] R.M. Caprioli, T.B. Farmer, J. Gile, Anal. Chem. 69 (1997) 4751.
[12] P.J. Todd, T.G. Schaaff, P. Chaurand, R.M. Caprioli, J. Mass Spectrom. 36 (2001) 355.
[13] P. Chaurand, S. Fouchecourt, B.B. DaGue, B.J. Xu, M.L. Reyzer, M.C. Orgebin-Crist, R.M. Caprioli, Proteomics 3 (2003) 2221.
[14] J. Pierson, J.L. Norris, H.R. Aerni, P. Svenningsson, R.M. Caprioli, P.E. Andren, J. Proteom. Res. 3 (2004) 289.
[15] M. Stoeckli, D. Staab, M. Staufenbiel, K.H. Wiederhold, L. Signor, Anal. Biochem. 311 (2002) 33.
[16] S.A. Schwartz, R.J. Weil, M.D. Johnson, S.A. Toms, R.M. Caprioli, Clin. Cancer Res. 10 (2004) 981.
[17] S.A. Schwartz, R.J. Weil, R.C. Thompson, Y. Shyr, J.H. Moore, S.A. Thoms, M.D. Johnson, R.M. Caprioli, Cancer Res. 65 (2005) 7674.
[18] K. Yanagisawa, Y. Shyr, B.J. Xu, P.P. Massion, P.H. Larsen, B.C. White, J.R. Roberts, M. Edgerton, A. Gonzalez, S. Nadaf, J.H. Moore, R.M. Caprioli, D.P. Carbone, Lancet 362 (2003) 433.
[19] S.S. Rubakhin, J.C. Jurchen, E.B. Monroe, J.V. Sweedler, Drug Discov. Today 10 (2005) 823.
[20] P. Chaurand, S.A. Schwartz, R.M. Caprioli, J. Proteom. Res. 3 (2004) 245.
[21] Y. Hsieh, R. Casale, E. Fukuda, J. Chen, I. Knemeyer, J. Wingate, R. Morrisson, W. Kormacher, Rapid Commun. Mass Spectrom. 20 (2006) 965.
[22] M.L. Reyzer, Y. Hsieh, K. Ng, W.A. Korfmacher, R.M. Caprioli, J. Mass Spectrom. 38 (2003) 1081.
[23] F.J. Troendle, C.D. Reddick, R.A. Yost, J. Am. Soc. Mass Spectrom. 10 (1999) 1315.
[24] R.J. Caldwell, R.M. Caprioli, Mol. Cell Proteom. 4 (2005) 394.
[25] A.C. Crecelius, D.S. Cornett, R.M. Caprioli, B. Williams, B.M. Dawant, B. Bodenheimer, J. Am. Soc. Mass Spectrom. 16 (2005) 1093.
[26] B. Franzen, Y. Yang, D. Sunnenmark, M. Wickmann, J. Ottervald, M. Oppermann, K. Sandberg, Proteomics 3 (2003) 1920.
[27] J.A. Maatta, E.T. Coffey, J.A. Hermonen, A.A. Salmi, A.E. Hinkkanen, Biochem. Biophys. Res. Commun. 238 (1997) 498.
[28] S. Shu, G. Ju, L.Z. Fan, Neurosci. Lett. 84 (1988) 169.
[29] K. Franklin, G. Paxinos, The Mouse Brain in Stereotaxic Coordinates, 2001, second ed., Academic Press, San Diego, 1997.
[30] R.H. Woodruff, R.J.M. Franklin, Glia 25 (1999) 216.

[31] S. Clerens, R. Ceuppens, L. Arckens, Rapid Commun. Mass Spectrom. 20 (2006) 3061.
[32] H.R. Aerni, D.S. Cornett, R.M. Caprioli, Anal. Chem. 78 (2006) 827.
[33] P. Chaurand, R.M. Caprioli, Electrophoresis 23 (2002) 3125.
[34] A.E. Palma, P. Owh, C. Frederic, C. Readhead, M.A. Moscarello, J. Neurochem. 69 (1997) 1753.
[35] A. Liu, C. Stadelmann, M. Moscarello, W. Bruck, A. Sobel, F.G. Mastronardi, P. Casaccia-Bonnefil, J. Neurosci. 25 (2005) 737.
[36] Lucchinetti, W. Bruck, J. Parisis, B. Scheithauer, M. Rodriguez, H. Lassmann, Ann. Neurol. 47 (2000) 707.
[37] B. Kornek, H. Lassmann, Brain Res. Bull. 15 (2003) 321.
[38] C. Alt, K. Duvefelt, B. Franzen, Y. Yang, B. Engelardt, Brain Pathol. 15 (2005) 1.
[39] G. Harauz, N. Ishiyama, C.M.D. Hill, I.R. Bates, D.S. Libich, C. Farès, Micron 35 (2004) 503.